

1

[ATLAS Semivisible Jets]

2

[Elena Laura Busch]

3

Submitted in partial fulfillment of the
requirements for the degree of
Doctor of Philosophy
under the Executive Committee
of the Graduate School of Arts and Sciences

4

5

6

7

8

COLUMBIA UNIVERSITY

9

2024

10

© 2024

11

[Elena Laura Busch]

12

All Rights Reserved

13

Abstract

14

[ATLAS Semivisible Jets]

15

[Elena Laura Busch]

16

Abstract of dissertation (place-holder).

Table of Contents

18	Acknowledgments	vii
19	Dedication	viii
20	Introduction or Preface	1
21	Chapter 1: The Standard Model	2
22	1.1 Phenomenology: Particles and Forces	2
23	1.1.1 Particles	2
24	1.1.2 Forces	3
25	1.2 QCD and Jets	6
26	1.3 Symmetries	7
27	1.3.1 Spontaneous Symmetry Breaking	8
28	1.4 Experimental Validation of the Standard Model	8
29	1.5 Limitations of the Standard Model	9
30	Chapter 2: Physics Beyond the Standard Model	11
31	2.1 Hidden Valley Theories	11
32	2.2 Semi-visible Jets	11
33	Chapter 3: The Large Hadron Collider	12

34	3.1 Accelerator Physics	13
35	3.1.1 The Journey of a Proton	13
36	3.1.2 Magnets	14
37	3.2 Luminosity	15
38	3.3 LHC Timeline	18
39	Chapter 4: The ATLAS Detector	20
40	4.1 Coordinate System and Geometry	20
41	4.2 Inner Detector	22
42	4.2.1 Pixel Detector	22
43	4.2.2 Semiconductor Tracker	23
44	4.2.3 Transition Radiation Tracker	23
45	4.3 Calorimeters	24
46	4.3.1 Liquid Argon Calorimeter	25
47	4.3.2 Tile Calorimeter	28
48	4.4 Muon Spectrometer	29
49	4.5 Magnet System	31
50	4.6 Forward Detectors	32
51	4.7 Trigger and Data Acquisition	33
52	Chapter 5: Particle Reconstruction and Identification	35
53	Conclusion or Epilogue	36
54	References	40

55	Appendix A: Experimental Equipment	42
56	Appendix B: Data Processing	43

List of Figures

58	1.1	Diagram of the 17 particles comprising the Standard Model	3
59	1.2	Fundamental interactions of the three fundamental forces described by the Stan-	
60		dard Model [1].	5
61	1.3	An example Feynmann diagram of jet production	6
62	3.1	The LHC accelerator complex at CERN [12]	14
63	3.2	The octants of the LHC and location of various beam activities [11]. Stars indi-	
64		cate the locations of beam collisions, and the associated detectors recording the	
65		outcome of those collisions.	15
66	3.3	(Left) Total integrated luminosity over the course of Run 2. (Right) Average num-	
67		ber of pp interactions per bunch crossing in Run 2. Each curve is weighted by the	
68		integrated luminosity for the year.	17
69	3.4	Timeline of LHC and HL-LHC activities [14]. Integrated luminosity estimates are	
70		approximate, and not reflective of the exact amount delivered to each experiment. .	19
71	4.1	ATLAS coordinate system and geometry	22
72	4.2	A 3D visualization of the structure of the ID in the barrel region [18]	23
73	4.3	ATLAS calorimetery system [19]	24
74	4.4	Diagram of a segment of the EMB, demonstrating the accordion plate arrangement	
75		[20]	26
76	4.5	A LAr pulse as produced in the detector (triangle) and after shaping (curve) [20] .	27
77	4.6	Readout gap structure in HEC [20]	27

78	4.7 TileCal wedge module [23]	29
79	4.8 Cross section view of the muon spectrometer system [24]	30
80	4.9 Layout of the barrel and endcap toroid magnets [17]	32

List of Tables

82

Acknowledgements

83 Insert your acknowledgements text here. This page is optional, you may delete it if not
84 needed.

85

Dedication

86

Dedicated to my friends and family

87

Introduction or Preface

88 Insert your preface text here if applicable. This page is optional, you may delete it if not
89 needed. If you delete this page make sure to move page counter comment in thesis.tex to correct
90 location.

91

92

Chapter 1: The Standard Model

93 The Standard Model of particle physics is a universally accepted framework which explains
94 the interactions of fundamental particles. All known fundamental particles, outlined in Figure 1.1,
95 are represented in the Standard Model. The model describes three of the four known fundamental
96 forces: the electromagnetic interaction, the weak interaction, and the strong interaction. Gravity,
97 the fourth fundamental force, is not addressed by the Standard Model (see more on this in section
98 1.5). The Standard Model was primarily developed over the course of the 1960s and 1970s, by
99 combining the work of many physicists into one coherent model. The Standard Model has been
100 established as a well-tested theory by decades of physics research.

101 This chapter will seek to introduce the phenomenology and mathematical foundations of the
102 Standard Model, and present the supporting experimental evidence. Phenomenon which are unex-
103 plained by the Standard Model will be considered at the end of the chapter, leading to an explo-
104 ration of theories beyond the Standard Model in the subsequent chapter.

105 **1.1 Phenomenology: Particles and Forces**

106 **1.1.1 Particles**

107 A classic representation of the particles comprising the Standard Model is shown in Figure 1.1.
108 The two primary particles classes are bosons (gauge bosons and the Higgs boson) and fermions
109 (leptons and quarks). The bosons are carriers of fundamental forces, while the fermions are the
110 building blocks of matter.

111 Each entry is accompanied by 3 characteristic numbers: mass, charge, and spin. The mass of
112 each particle is determined to limited precision by experimental observation, with the exception of
113 photons and gluons which are known to be massless. Charge refers to the familiar electromagnetic

Standard Model of Elementary Particles

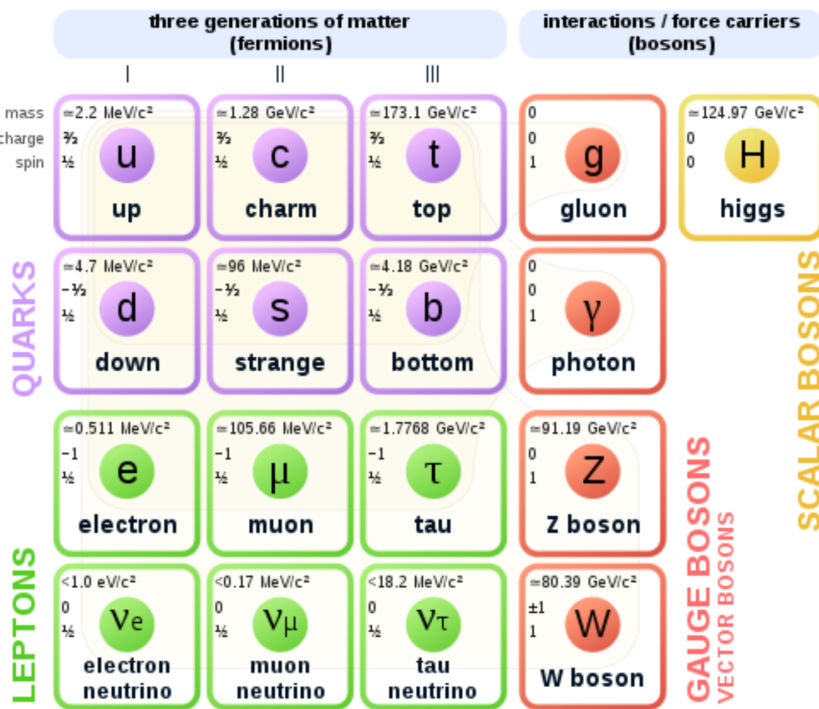


Figure 1.1: Diagram of the 17 particles comprising the Standard Model

114 charge in the case of leptons, W and Z bosons, and to color charge in the case of quarks and gluons.

115 Spin is an intrinsic form of angular momentum carried by fundamental particles; all fermions have
116 half integer spin, while bosons have integer spin.

117 Fermions come in flavor families

118 Each particle is also known to have an *antiparticle*. Each antiparticle has the same mass but the
119 opposite charge of their Standard Model counter part; for example, the antiparticle of the electron
120 is the positron, which has all the same properties but a positive charge. The photon, Z boson,
121 and Higgs are all their own antiparticle. The nature of antineutrinos is an open question driving
122 neutrino physics research, as it is not currently known whether neutrinos are their own antiparticle.

1.1.2 Forces

124 The three fundamental forces explained by the Standard Model are the electromagnetic force,
125 the strong force, and the weak force. The photon is the carrier of the electromagnetic force, which

126 dictates the nature of interactions between electrically charged particles, and is widely covered by
127 introductory physics courses. The electromagnetic force has an infinite interaction range, a result
128 of the massless and non-self interaction nature of the photon. The electromagnetic interaction is
129 described by the theory of quantum electrodynamics (QED).

130 The weak force gives rise to atomic radiation and decay. It allows for the processes of beta
131 decay and electron capture, which enable protons to convert to neutrons, and vice-versa, within
132 the nucleus of an atom. In the process of beta decay, a proton decays into a neutron, a positron,
133 and a neutrino; or, a neutron decays into a proton, an electron and an antineutrino. The weak
134 interaction also plays a roll in the processes of nuclear fusion and nuclear fission. The W^+ , W^- ,
135 and Z^0 are the force carriers of the weak force. The effective range of the weak force is limited to
136 subatomic distances, as a result of the massive nature of the mediator bosons. The unified theory
137 of the electroweak interaction posits that at high enough energies the electromagnetic interaction
138 and the weak force merge into the same force. This threshold is termed the unification energy and
139 estimated to be around 246 GeV.

140 The strong force confines quarks into hadron particles, such as protons and neutrons. The
141 strong force also allows for the creation of atomic nuclei by binding protons and neutrons together,
142 and is generally referred to as the “nuclear force” in this context. The gluon is the mediator of the
143 strong force, which is a short-range force which acts at subatomic distances on the order of 10^{-15}
144 m. At this range, the strong force is about 100x as strong as the electromagnetic force, which
145 allows for the creation of positively charged nuclei [**griffiths**]. The strong force is described by the
146 theory of quantum chromodynamics (QCD). In the same way that QED dictates the interaction of
147 electrically charges particles, QCD dictates the interactions of *color-charged* particles. Due to the
148 particular importance of QCD in this thesis, this topic will be explored in detail in section 1.2.

149 The fundamental Feynmann diagram for each of the three forces discussed here is depicted
150 in Figure 1.2. The fourth fundamental force, gravity, is not currently explained by any known
151 mechanism within the Standard Model.

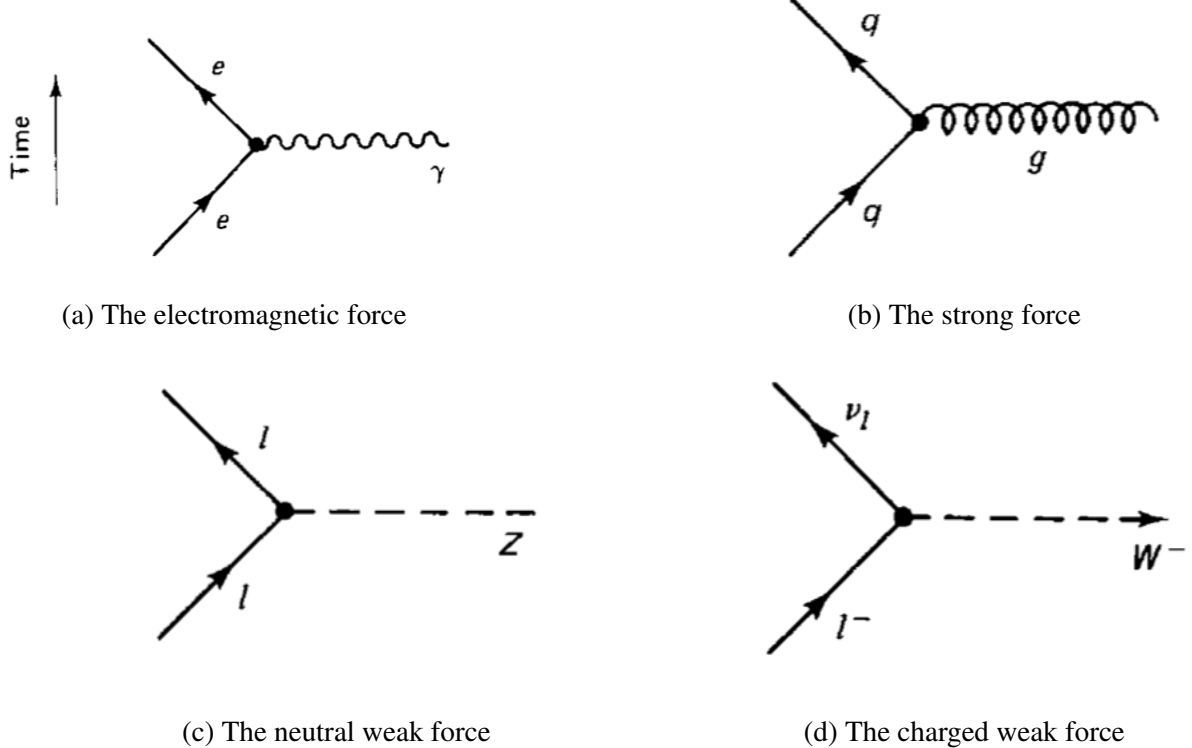


Figure 1.2: Fundamental interactions of the three fundamental forces described by the Standard Model [1].

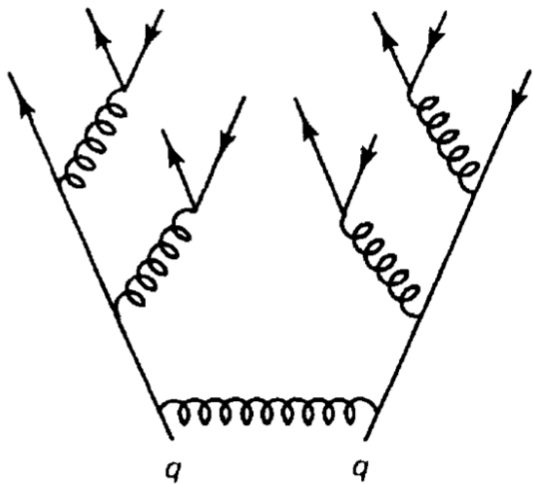


Figure 1.3: An example Feynmann diagram of jet production

¹⁵² **1.2 QCD and Jets**

¹⁵³ The role of color in QCD at the surface level is analogous to that of electric charge in QED.
¹⁵⁴ However, while there is only one type of electric charge, there are three types of color charge -
¹⁵⁵ red, green, and blue. In the process $q \rightarrow q + g$, the color of the quark can change. In order to
¹⁵⁶ conserve color charge, gluons are bicolored, and always carry positive color charge and negative
¹⁵⁷ color charge.

¹⁵⁸ Color charged particles only exist in bound states which result in a neutral total color charge, a
¹⁵⁹ principle known as confinement. This requires that quarks and gluons exist in group states known
¹⁶⁰ as hadrons; either mesons in the case of two quarks or baryons in the case of three quarks. When
¹⁶¹ a quark is separated from a hadron, confinement dictates that other colored objects are produced
¹⁶² around the quark to obey confinement. An example of this process is shown in Figure 1.3This
¹⁶³ ensemble of objects, generally a mixture of quarks and gluons, is termed a *jet*. Jets are among the
¹⁶⁴ most common phenomenon observed by particle detectors at hadron colliders.

165 **1.3 Symmetries**

166 The Standard Model is a renormalizable quantum field theory that obeys the local symmetry

167 G_{SM} :

$$G_{SM} = SU(3)_C \times SU(2)_L \times U(1)_Y. \quad (1.1)$$

168 The $SU(3)_C$ symmetry component represents the non-Abelian gauge group of QCD. There are
169 8 generators for the $SU_C(3)$ group which correspond to the 8 types of gluon [2].

170 The $SU(2)_L \times U(1)_Y$ symmetry group represents the electroweak sector of the Standard Model,
171 which can be spontaneously broken into the electromagnetic and weak sectors. There are 4 gen-
172 erators for this group, which correspond to the four massless gauge bosons W^1 , W^2 , W^3 , and B .
173 From these massless gauge bosons are formed the massive mediators of the weak force, the W^- ,
174 W^+ and Z^0 bosons, and the massless electromagnetic force carrier, the photon γ .

175 Noether's theorem stipulates that any continuous symmetry is associated with a conserved
176 quantity. In the Standard Model, this means that the $SU(3)_C$ symmetry gives rise to conservation
177 of color charge. The $SU(2)_L \times U(1)_Y$ symmetry gives rise to conservation of electromagnetic
178 charge via symmetry breaking, which will be discussed in greater detail below. Conservation
179 of spin results from the Poincaré symmetry described by the theory of special relativity, which
180 combined with Noether's theorem gives us the conversation of energy, momentum, and angular
181 momentum.

182 The SM Lagrangian is invariant under CPT symmetry, or charge, parity, and time reversal.
183 Charge conjugation (C) transform a particles into it's corresponding antiparticle by reversing the
184 charge and other quantum numbers. Parity conjugation (P) reverses spatial coordinates, which
185 transforms left-handed particles into right-handed particles and vice-versa. Time reversal (T) is
186 the theoretical process of reversing time. The L subscript in the $SU(2)_L$ group indicates that this
187 symmetry only applies to the left-handed components of fermions. As a result, the $W^{1,2,3}$ generator
188 bosons of $SU(2)_L$ only interact with left handed particles, a process which violates CP symmetry.

¹⁸⁹ The CPT theorem states that the violation of CP symmetry implies that T-symmetry must also be
¹⁹⁰ violated, so that *CPT* is a preserved symmetry.

¹⁹¹ 1.3.1 Spontaneous Symmetry Breaking

¹⁹² Higgs field a scalar field that forms a complex doublet of SU(2)

¹⁹³ Spontaneous symmetry breaking is the process by which a Lagranian obeys a symmetry at
¹⁹⁴ high energies, but exhibits asymmetric behavior at lower energies. The electroweak symmetry
¹⁹⁵ group is spontaneously broken as $SU(2)_L \times U(1)_Y \rightarrow U(1)_{EM}$. The quantity conserved by the
¹⁹⁶ $SU(2)_L$ symmetry is weak isospin $T_{1,2,3}$, while the quantity conserved by $U(1)_Y$ symmetry is weak
¹⁹⁷ hypercharge Y . Below very high energies, the presence of the Higgs field causes the electroweak
¹⁹⁸ symmetry to break. This causes the four massless gauge bosons ($W^{1,2,3}$ and B) to mix, resulting
¹⁹⁹ in the massive gauge bosons W^- , W^+ and Z^0 bosons and the massless photon γ . The Higgs
²⁰⁰ mechanism allows the W^\pm and Z bosons to be massive. The symmetry breaking also violates
²⁰¹ the conservation of weak isospin and weak hypercharge, leaving only electromagnetic charge $Q =$
²⁰² $T_3 + \frac{1}{2}Y$ as a conserved quantity associated with the $U(1)_{EM}$ symmetry.

²⁰³ 1.4 Experimental Validation of the Standard Model

²⁰⁴ TODO: add citations for all original discoveries.

²⁰⁵

²⁰⁶ The theoretical framework of the Standard Model coalesced into a unified theory in the mid-
²⁰⁷ 20th century. A cascade of discoveries providing empirical evidence for the model followed
²⁰⁸ closely. In the 1960s, three quarks (up, down and strange) and four leptons (electron, muon,
²⁰⁹ and their associated neutrinos) were the known particulate building blocks of matter and the Stan-
²¹⁰ dard Model. The discovery of the charm quark in 1974, through the observation of the J/ψ me-
²¹¹ son [3][4], confirmed the existence of a fourth quark flavor and explained the absence of flavor-
²¹² changing neutral currents [1]. The discovery of the τ in 1975 [5] provided the first evidence of a
²¹³ 3rd generation of matter. This was quickly followed by the observation of the Υ meson in 1977,

214 which provided evidence for the existence of a fifth quark, the b bottom quark (sometimes also
215 referred to as the beauty quark). The existence of a 3rd generation of fermion also explained the
216 observation of CP violation in the weak force, as it allows for the appearance of a complex phase in
217 the CKM matrix. The t top quark and ν_τ tau neutrino were predicted at this point as the final build-
218 ing blocks of three complete generations of fermions, and they were discovered by experimental
219 observation around the turn of the 21st century.

220 The W and Z bosons were predicted by the Standard Model, but to observe them required
221 the construction of a particle accelerator powerful enough to produce them. They were finally
222 observed at CERN in 1983 by the UA1 and UA2 experiments at the newly constructed Super Proton
223 Synchrotron (SPS). Their masses were observed to be compatible with those predicted by the
224 Standard Model nearly a decade earlier. The final missing piece then was confirming the existence
225 of the Higgs, which again required the construction of a newer and more powerful collider. CERN
226 achieved this with the construction of the Large Hadron Collider (LHC), and in 2012 the ATLAS
227 and CMS experiments announced the discovery of the Higgs particle.

228 **1.5 Limitations of the Standard Model**

229 TODO: add citations for all phenomenon.

230

231 While the Standard Model has enjoyed decades of experimental results which confirm its pre-
232 dictions, there are several glaring shortcomings. The observed phenomenon for which the Standard
233 Model provides no explanation are summarized below.

- 234 • Gravity - the Standard Model does not account for the fourth fundamental force of gravity.
- 235 • Dark Matter - there is no viable candidate to explain the existence of dark matter, a non-
236 interacting form of matter which must exist to account for gravitational observations which
237 cannot be explained by general relativity, such as the motion of galaxies, gravitational lens-
238 ing, and the structure of the universe.

239 • Matter-Antimatter asymmetry - the level of CP violation in the Standard Model isn't suf-
240 ficient to explain the large discrepancy between the amount of matter and the amount of
241 antimatter in the universe today, and the origins of this imbalance are not understood.

242 • Neutrino masses - the Standard Model assumes that neutrinos are massless and provides
243 no mechanism for them to acquire mass. However, observations of neutrino oscillations
244 indicates they posses some very small but non-zero mass.

245 In additional to these unexplained natural phenomenon, there are several questions about the
246 *naturalness* of the Standard Model. The principle of naturalness states that dimensionless ratios
247 between physical constants should be of order 1, and that nature should not be arbitrarily fine-
248 tuned. While this is largely an aesthetic argument, it points to many aspects of the Standard Model
249 for which there exists no natural explanation.

250 • Strong CP - while CP symmetry is violated in the weak force, it appears to be preserved in
251 the strong force, although CP violation in the strong force is allowed by the SM. There is no
252 principle which motivates this incongruity between the weak force and strong force.

253 • Hierarchy Problem - The wide range of masses for elementary particles and the wide range of
254 scales at which the four fundamental forces operate is not motivated by the SM. Specifically,
255 it is not understood why the Higgs mass is observed to be well below the Plank scale λ ,
256 which is the energy level at which the effects of quantum gravity become significant. QFT
257 indicates that the Higgs mass is determined by contributions from all energy scales including
258 λ , which indicates that it's observed mass is inexplicably small.

259 These limitations of the Standard Model provide a road map for theoretical and experimental
260 particle physicists, who seek to develop new theories which account for these observations, and
261 then to find evidence which might support these *beyond the Standard Model* (BSM) theories. The
262 next chapter will introduce the BSM theories which motivate the physics search presented in this
263 thesis.

264

265

Chapter 2: Physics Beyond the Standard Model

266 **2.1 Hidden Valley Theories**

267 **2.2 Semi-visible Jets**

Chapter 3: The Large Hadron Collider

270 The Large Hadron Collider (LHC) is a 26.7 km circular high-energy particle accelerator, span-
 271 ning the Swiss-French border near the city of Geneva, Switzerland [6]. The LHC occupies the
 272 tunnel constructed in 1989 for the Large Electron-Positron (LEP) Collider, and reaches a maxi-
 273 mum depth of 170m below the surface. The LHC is operated by the European Organization for
 274 Nuclear Research (CERN), the largest international scientific collaboration in the world.

275 The LHC accelerates protons and heavy ions, and collides them at four interaction points
 276 around the ring, with a design center-of-mass energy per collision of $\sqrt{s} = 14$ TeV. Each interaction
 277 point is home to one of four detector experiments, which study the products of the collisions. The
 278 largest of these experiments is the ATLAS detector, a general purpose detector designed to study
 279 the Standard Model and search for new physics that could be produced in LHC collisions [7]. The
 280 CMS detector is another general purpose detector, designed and operated independently of the AT-
 281 LAS detector, but intended to probe the same range of physics [8]. The ALICE experiment is a
 282 dedicated heavy ion experiment, and the LHC-b experiment is a dedicated *b*-physics experiment
 283 [9] [10].

284 This chapter will cover the multi-component accelerator complex powering the LHC, the state-
 285 of-the-art magnets which steer the particle beams, measurements of the intensity and number of
 286 collisions produced by the LHC, and finally an overview of LHC activities in the past, present, and
 287 future.

288 **3.1 Accelerator Physics**

289 **3.1.1 The Journey of a Proton**

290 From 2010 - 2018, the protons which fed the LHC started as hydrogen gas. The electrons were
291 removed from the hydrogen atoms through the use of strong electric fields. The linear accelerator
292 LINAC2 then accelerated the protons to an energy of 50 MeV. Between 2018 and 2020, LINAC2
293 was replaced with LINAC4, which instead accelerates H^- ions, hydrogen atoms with two electrons.
294 LINAC4 is capable of accelerating the H^- ions to 160 MeV. Before injection to the next part of
295 the acceleration chain, both electrons are stripped from the H^- ions, leaving just protons. From
296 here the protons enter the Proton Synchrotron booster, where they are accelerated up to 1.4 GeV of
297 energy. Subsequently they are sorted into bunches separated in time by 25 ns, where each bunch
298 contains approximately 10^{11} protons. Next the bunches pass through the Proton Synchrotron (PS)
299 and the Super Proton Synchrotron (SPS), where they reach energies of 25 GeV and 450 GeV
300 respectively. Finally they are injected into the LHC as two beams traveling in opposite direction.
301 The original design allowed each beam to be accelerated up to 7 TeV of energy. Due to limitations
302 in the performance of the superconducting LHC magnets, the highest energy actually achieved by
303 the LHC beams during Run 2 was 6.5 TeV, giving a collision center-of-mass energy of $\sqrt{s} = 13$
304 TeV [11]. Figure 3.1 shows the full LHC accelerator complex.

305 Acceleration in the LHC is performed by eight radio frequency (RF) cavities located around the
306 ring. Each RF cavity produces a 2 MV electric field oscillating at 40 MHz. The 40MHz oscillation
307 produces a point of stable equilibrium every 2.5 ns. These points of equilibrium are synchronized
308 with the occurrence of the proton bunches produced in the PS – a proton bunch occupies one out
309 of every ten points of stable equilibrium, such that the bunches maintain a 25 ns spacing [11].

310

The CERN accelerator complex Complexe des accélérateurs du CERN

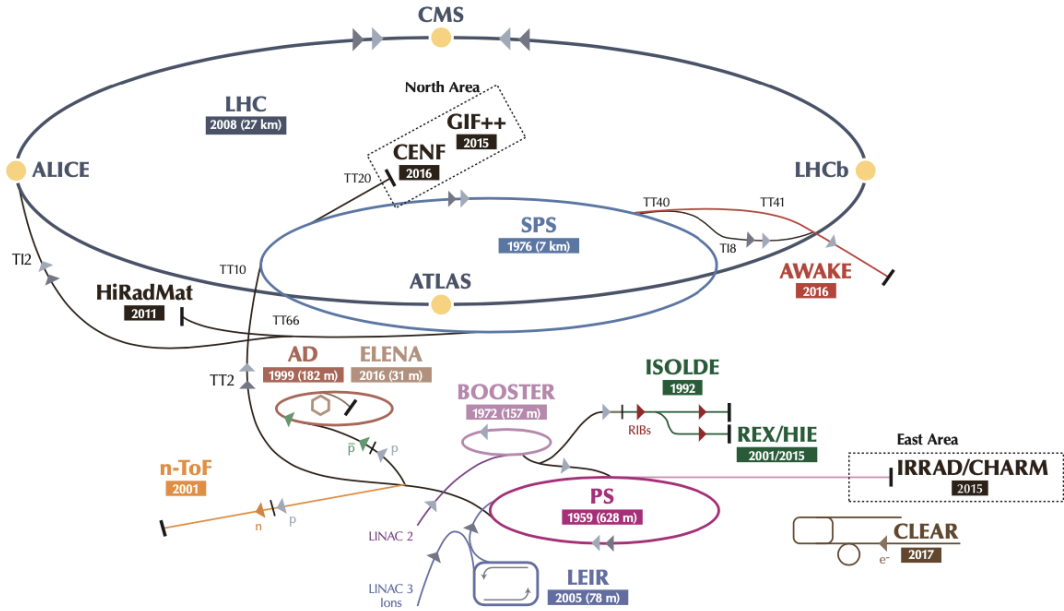


Figure 3.1: The LHC accelerator complex at CERN [12]

311 3.1.2 Magnets

312 In addition to the acceleration cavities, the LHC houses 9593 superconducting magnets which
 313 direct and focus the proton beam on its 27 kilometer journey. The magnets are comprised of super-
 314 conducting Niobium-Titanium coils cooled to 1.9K by superfluid helium. As the beams approach
 315 one of the four collision points around the ring, multipole magnets focus and squeeze the beam for
 316 optimal collisions [11].

317 The LHC is divided into sections, where each section contains an arc and a straight insertion. The arcs are composed of 1232 large dipole magnets which bend the beam
 318 to follow the roughly circular 27 km path. The main dipoles generate powerful 8.3 tesla magnetic
 319 fields to achieve this bend. Each dipole magnet is 15 meters long and weighs 35 tonnes. The
 320 dipoles work in conjunction with quadrupole magnets, which keep the particles in a focused beam,
 321 and smaller sextupole, octupole and decapole magnets which tune the magnetic field at the ends of
 322 the dipole magnets [13].

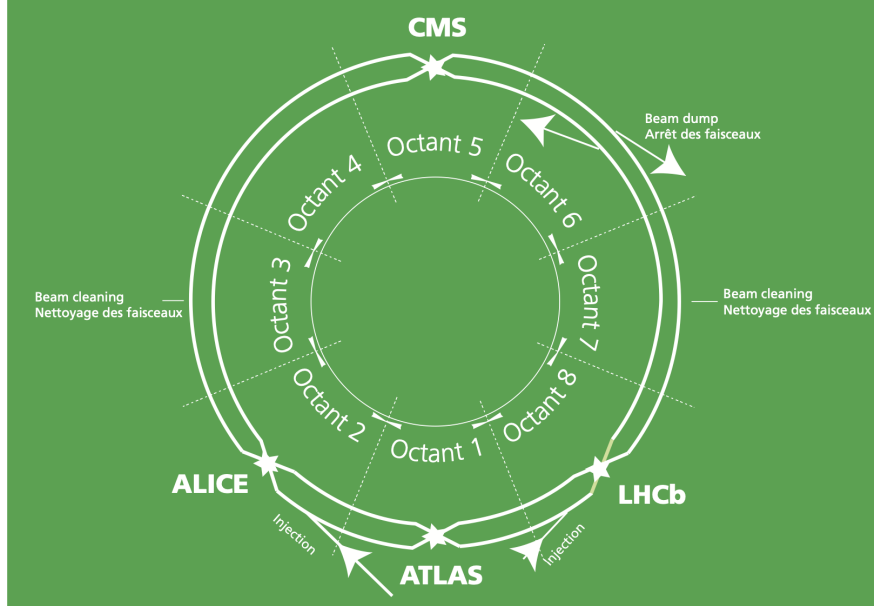


Figure 3.2: The octants of the LHC and location of various beam activities [11]. Stars indicate the locations of beam collisions, and the associated detectors recording the outcome of those collisions.

324 The straight insertion sections have different purposes depending on their location around the
 325 ring: beam collisions, beam injection, beam dumping, or beam cleaning. At the four collision
 326 points, insertion magnets squeeze the beam to ensure a highly focused collision. This is accom-
 327 plished with a triplet of quadrupole magnets, which tighten the beam from 0.2 millimeters to just
 328 16 micrometers in diameter. Insertion magnets also clean the beam, which prevents stray particles
 329 from hitting sensitive components throughout the LHC. When the LHC is ready to dispose of a
 330 beam of particles, beam dump magnets deflect the path of the beam into a straight line towards
 331 a block of concrete and graphite that stops the beam. A dilution magnet then reduces the beam
 332 intensity by a factor of 100,000 before the final stop [13]. Figure 3.2 shows the locations various
 333 beam activities.

334 3.2 Luminosity

335 Collisions at the LHC occur when the two beams of proton bunches cross at one of the four
 336 interaction points. The intensity of collisions is described by the instantaneous luminosity, the

337 formula for which is given in equation 3.1.

$$L = \frac{fN_1N_2}{4\pi\sigma_x\sigma_y} \quad (3.1)$$

338 Here f is the revolution frequency, N_1 and N_2 are the number of particle per bunch for each
339 beam, and σ_x , σ_y are the horizontal and vertical beam widths.

340 The instantaneous luminosity gives the number of the collisions that could be produced at the
341 interaction point per unit of cross-sectional area per unit of time, generally expressed in $\text{cm}^{-2}\text{s}^{-1}$.
342 The integrated luminosity is obtained by integrating the instantaneous luminosity over a given
343 block of time, and measures the total number of collisions which have occurred during that op-
344 eration period. The total integrated luminosity is directly correlated with the size of the datasets
345 collected by the LHC experiments. Total integrated luminosity for Run 2 is illustrated in Figure
346 3.3.

347 High levels of instantaneous luminosity result in multiple pp collisions per bunch crossing,
348 which leads to an effect known as *pileup*. Pileup poses a challenge for detector physics, as recon-
349 structing the products of multiple simultaneous events is far more challenging than reconstructing
350 a single event with no pileup. Pileup conditions vary from year-to-year and run-to-run of LHC op-
351 eration, and the impact of these conditions are taken into account when analyzing the data, as will
352 be discussed further in Chapter 5. Measurement of pileup conditions during Run 2 are illustrated
353 in Figure 3.3.

354 The design peak luminosity of the LHC is $1.0 \times 10^{34} \text{ cm}^{-2}\text{s}^{-1}$. During Run 1 of the LHC the
355 peak instantaneous luminosity was $0.8 \times 10^{34} \text{ cm}^{-2}\text{s}^{-1}$. Over the course of Run 1 the LHC collected
356 a total integrated luminosity of 5.46 fb^{-1} at $\sqrt{s} = 7 \text{ TeV}$, and 22.8 fb^{-1} at $\sqrt{s} = 8 \text{ TeV}$. Following the
357 first long shutdown and upgrade phase of operations, the LHC achieved a center of mass energy
358 $\sqrt{s} = 13 \text{ TeV}$ at the beginning of Run 2 in 2015. The LHC was also able to deliver 2.0×10^{34}
359 $\text{cm}^{-2}\text{s}^{-1}$ peak instantaneous luminosity, double the design value. During LHC Run 2, from 2015-
360 2018, the LHC delivered 156 fb^{-1} of integrated luminosity for proton-proton collisions. Run 3 of

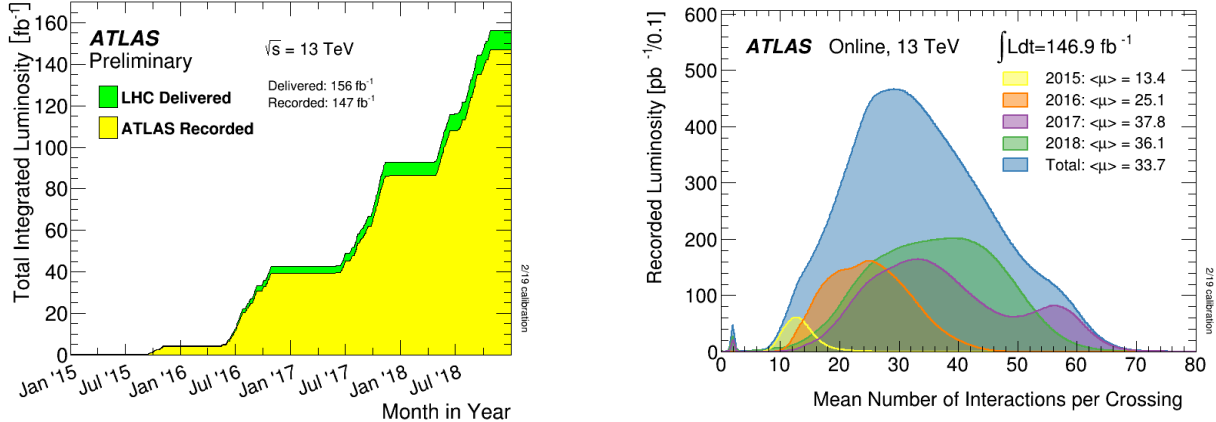


Figure 3.3: (Left) Total integrated luminosity over the course of Run 2. (Right) Average number of pp interactions per bunch crossing in Run 2. Each curve is weighted by the integrated luminosity for the year.

361 the LHC began in 2022, and is expected to deliver 250 fb^{-1} of integrated luminosity to the ATLAS
 362 and CMS experiments by 2026 [14].

363 The goal of LHC physic analyses is to find and study rare events produced by interesting
 364 physics processes. The cross section σ of a given process indicates the probability of that process
 365 occurring given the beam conditions of the LHC. Multiplying the cross section by the integrated
 366 luminosity of a dataset gives the expected number of events for that process within the dataset.

$$N_{\text{events}} = \int \sigma L(t) dt = \mathcal{L} \times \sigma \quad (3.2)$$

367 The cross section for most processes of interest, especially BSM processes, is several orders of
 368 magnitude below the total cross section for the LHC. Therefore maximizing the number of events
 369 produced in collisions is crucial to increase the likelihood of producing events from processes of
 370 interest. For this reason, maximizing instantaneous luminosity is a key factor in accelerator design
 371 and operation, while mitigating the resulting pileup effects is a key component in detector design
 372 and operation.

373 **3.3 LHC Timeline**

374 The first proton-proton collisions at the LHC were achieved in 2010 with a center-of-mass
375 energy of $\sqrt{s} = 7$ TeV. Run 1 of the LHC took place between 2010 and early 2013, during which
376 time the center-of-mass collision energy increased from 7 TeV to 8 TeV. Figure 3.4 shows an
377 overview of LHC activities beginning in 2011, in the midst of Run 1. The data collected during
378 Run 1 led to the discovery of the Higgs Boston in 2012 [15].

379 Between 2013 and 2015 the LHC underwent the first Long Shutdown (LS1) during which
380 time maintenance and renovation was performed on the accelerator chain, including the repair and
381 consolidation of the high-current splices which connect the super-conducting LHC magnets. Run
382 2 of the LHC took place from 2015 to 2018 and achieved a center-of-mass energy of $\sqrt{s} = 13$ TeV.
383 Analysis of data collected in Run 2 is still on going, and is the subject of study in this thesis.

384 Between 2018 and 2022 the LHC underwent the second Long Shutdown (LS2), allowing for
385 further detector and accelerator maintenance and upgrades. Key improvements to the LHC in-
386 cluded the improvement of the insulation for over 1200 diode magnets, and the upgrade from
387 LINAC2 to LINAC4 mentioned in Section 3.1.1. Run 3 of the LHC began in 2022 and achieved a
388 center-of-mass energy of $\sqrt{s} = 13.6$ TeV.

389 Run 3 is scheduled to continue through 2026, at which point the LHC machine and detectors
390 will undergo upgrades for the *high luminosity* LHC (HL-LHC). The HL-LHC will increase the
391 instantaneous machine luminosity by a factor of 5 - 7.5 with respect to the nominal LHC design.
392 The bottom panel of Figure 3.4 shows an overview of the preparation work for the HL-LHC that
393 has been going on concurrently with Run 1, 2, and 3 of the LHC [16].



Figure 3.4: Timeline of LHC and HL-LHC activities [14]. Integrated luminosity estimates are approximate, and not reflective of the exact amount delivered to each experiment.

Chapter 4: The ATLAS Detector

396 The ATLAS detector (**A** Toroidal **L**H**C** Apparatu**S**) is one of two general purpose physics
 397 detectors designed to study the products of proton-proton collisions at the LHC. The detector is
 398 composed of a variety of specialized subsystems, designed to fully capture a wide array of physics
 399 processes. The apparatus is 25m high, 44m in length, and weighs over 7000 tons [17]. The LHC
 400 beam pipes direct proton beams to an interaction point at the center of ATLAS, and the cylindrical
 401 detector design captures a complete 360° view of the *event*, tracking all particles that result from
 402 the collision.

403 The main components of the ATLAS detector are the Inner Detector (ID) which provides high
 404 precision tracking of charged particles leaving the collision vertex, the calorimeter system which
 405 measures the energy of electromagnetic and hadronic objects, and the Muon Spectrometer (MS)
 406 which gives detailed information about muons that reach the outer radii of the detector. Two
 407 magnet systems, a 2 T solenoid magnet surrounding the ID, and a 0.5-1.0 T toroid magnet system
 408 situated throughout the MS, produce magnetic fields which bend the trajectory of charged particles
 409 traversing the detector. In addition to the main detector components, dedicated forward detectors
 410 monitor beam conditions and instantaneous luminosity, and an online trigger system reduces the
 411 data rate to a manageable level for storage. Each of these components will be discussed in further
 412 detail in this chapter.

413 **4.1 Coordinate System and Geometry**

414 The ATLAS detector employs a right hand cylindrical coordinate system. The z axis is aligned
 415 with the beam line, and the x-y plane sits perpendicular to the beam line. The coordinate system
 416 origin is centered on the detector, such that the origin corresponds with the interaction point of the

417 two colliding beams. The detector geometry is usually characterized by polar coordinates, where
418 the azimuthal angle ϕ spans the x-y plane. The polar angle θ represents the angle away from the
419 beam line, or z axis. $\theta = 0$ aligns with the positive z -axis, and $\phi = 0$ aligns with the positive x-axis.

420 The polar coordinate θ is generally replaced by the Lorentz invariant quantity *rapidity* or y :

$$y = \frac{1}{2} \ln\left(\frac{E + p_z}{E - p_z}\right). \quad (4.1)$$

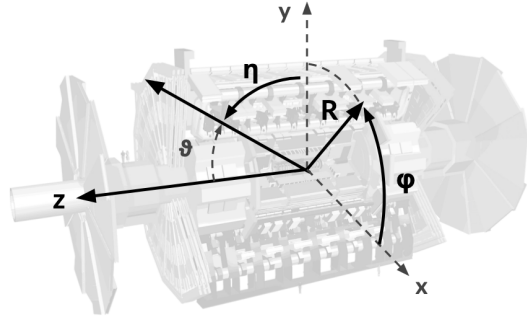
421 This substitution is advantageous because objects in the detector are traveling at highly rela-
422 tivistic speeds. The relativistic speed also means that the masses of the particles are generally small
423 compared to their total energy. In the limit of zero mass, the rapidity y reduces to the pseudorapid-
424 ity η , which can be calculated directly from the polar angle θ :

$$\eta = -\ln\left(\frac{\theta}{2}\right). \quad (4.2)$$

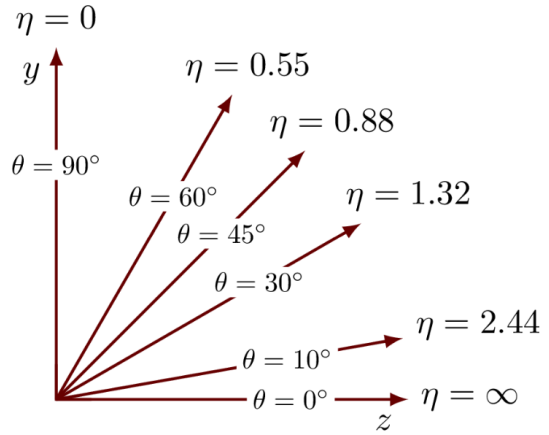
425 The distance between physics objects in the detector is generally expressed in terms of the solid
426 angle between them ΔR :

$$\Delta R = \sqrt{\Delta\phi^2 + \Delta\eta^2} \quad (4.3)$$

427 Figure 4.1a depicts the orientation of the coordinate system with respect to the ATLAS detector,
428 while Figure 4.1b illustrates the relationship between θ , η , and the beamline axis z . Direct or “head
429 on” proton-proton collisions are more likely to result in objects whose momentum is directed
430 along transverse plane (low $|\eta|$); glancing proton-proton collisions are more likely to result in
431 objects whose momentum is directed along the z -axis (high $|\eta|$). Due to the difference in the
432 nature of these collisions, as well as the cylindrical design of the ATLAS detector, the detector
433 is divided into regions of low and high η . Each subsystem has a “central” or “barrel” region
434 covering low $|\eta|$, while the “forward” or “end-cap” regions cover the area up to $|\eta| = 4.9$. Each of
435 the three main ATLAS subsystems will be discussed in the following sections.



(a) The ATLAS geometry



(b) Relationship between η and θ

Figure 4.1: ATLAS coordinate system and geometry

436 4.2 Inner Detector

437 The Inner Detector (ID) is the ATLAS subsystem closest to the interaction point. The primary
 438 purpose of the ID is to determine the charge, momentum, and trajectory of charged particles pass-
 439 ing through the detector. With this information the ID is also able to precisely determine interaction
 440 vertices.

441 The ID is composed of three sub-detectors; the Pixel Detector, the Semiconductor Tracker
 442 (SCT) and the Transition Radiation Tracker (TRT). Figure 4.2 shows the location of these three
 443 subsystems with respect to each other and the interaction point.

444 4.2.1 Pixel Detector

445 The pixel detector is the first detector encountered by particles produced in LHC collisions.
 446 The original pixel detector consists of 3 barrel layers of silicon pixels, positioned at 5 cm, 9 cm
 447 and 12 cm from the beamline. There are also 3 disks on each end-cap positioned 50 - 65 cm from
 448 the interaction point, providing full coverage for $|\eta| < 2.2$. The layers are comprised of silicon
 449 pixels each measuring $50 \times 400 \mu\text{m}^2$, with 140 million pixels in total. The pixels are organized
 450 into modules, which each contain a set of radiation hard readout electronics chips. In 2014, the
 451 Insertable B-layer (IBL) was installed, creating a new innermost layer of the pixel detector sitting

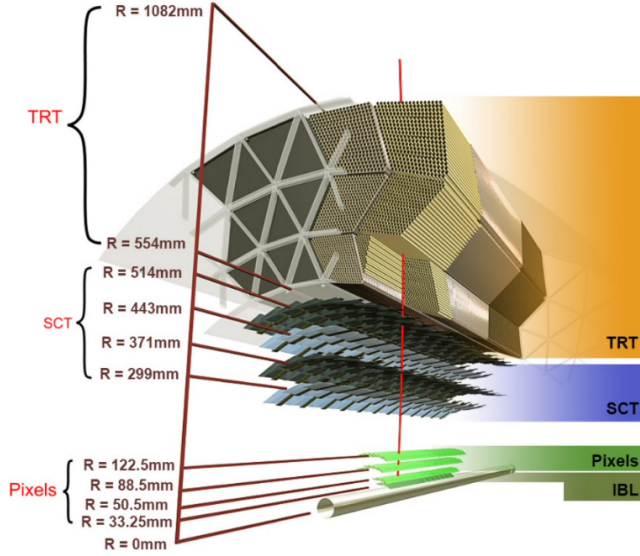


Figure 4.2: A 3D visualization of the structure of the ID in the barrel region [18]

452 just 3.3 cm from the beamline. The pixels of the IBL measure $50 \mu\text{m}$ by $250 \mu\text{m}$, and cover
 453 a pseudo-rapidity range up to $|\eta| < 3$. The IBL upgrade enhances the pixel detector's ability
 454 to reconstruct secondary vertices associated with short-lived particles such as the b-quark. The
 455 improved vertex identification also helped compensate for increasing pile-up in Run 2 [17].

456 4.2.2 Semiconductor Tracker

457 The SCT provides at least 4 additional measurements of each charged particle. It employs the
 458 same silicon technology as the Pixel Detector, but utilizes larger silicon strips which measure $80 \mu\text{m}$
 459 by 12.4 cm . The SCT is composed of 4 barrel layers, located between 30 cm and 52 cm from
 460 the beamline, and 9 end-cap layers on each side. The SCT can distinguish tracks that are separated
 461 by at least $200 \mu\text{m}$.

462 4.2.3 Transition Radiation Tracker

463 The TRT provides an additional 36 hits per particle track. The detector relies on gas filled
 464 straw tubes, a technology which is intrinsically radiation hard. The straws which are each 4 mm in
 465 diameter and up to 150 cm in length and filled with xenon gas. The detector is composed of about

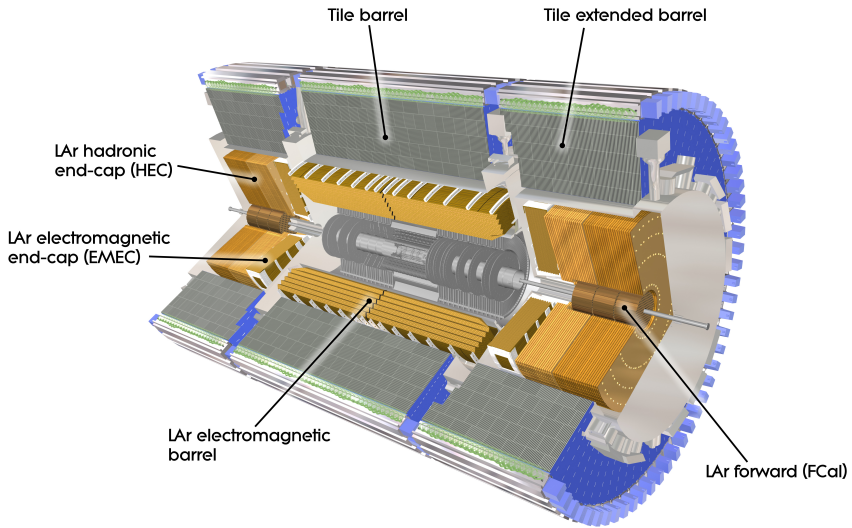


Figure 4.3: ATLAS calorimetry system [19]

466 50000 barrel region straws and 640000 end-cap straws, comprising 420000 electronic readout
 467 channels. Each channel provides a drift time measurement with a spatial resolution of $170\text{ }\mu\text{m}$ per
 468 straw. As charged particles pass through the many layers of the detector, transition radiation is
 469 emitted. The use of two different drift time thresholds allows the detector to distinguish between
 470 tracking hits and transition radiation hits.

471 4.3 Calorimeters

472 The ATLAS calorimeter system is responsible for measuring the energy of electromagnetically
 473 interacting and hadronically interacting particles passing through the detector. The calorimeters are
 474 located just outside the central solenoid magnet, which encloses the inner detectors. The calorime-
 475 ters also stop most known particles, which the exception of muons and neutrinos, preventing them
 476 from traveling to the outermost layers of the detector. The ATLAS calorimetry system is composed
 477 of two subsystems - the Liquid Argon (LAr) calorimeter for electromagnetic calorimetry and the
 478 Tile calorimeter for hadronic calorimetry. The full calorimetry system is shown in Figure 4.3.

479 4.3.1 Liquid Argon Calorimeter

480 The LAr calorimeter is a sampling calorimeter designed to trigger on and measure the ener-
481 gies of electromagnetic (EM) particles, as well as hadronic particles in the high η regions. It is
482 divided in several regions, as shown in Figure 4.3. For the region $|\eta| < 1.4$, the electromagnetic
483 barrel (EMB) is responsible for EM calorimetry, and provides high resolution energy, timing,
484 and position measurements for electrons and photons passing through the detector. The elec-
485 tromagnetic endcap (EMEC) provides additional EM calorimetry up to $|\eta| < 3.2$. In the re-
486 gion $1.4 < |\eta| < 3.2$, the hadronic endcap (HEC) provides hadronic calorimetry. For hadronic
487 calorimetry in the region $|\eta| < 1.4$, corresponding to a detector radii > 2.2 m, the less expensive
488 tile calorimeter (discussed in the next section) is used instead. A forward calorimeter (FCAL)
489 extends the hadronic calorimetry coverage up to $3.1 < |\eta| < 4.8$ [20].

490 The LAr calorimeter is composed of liquid argon sandwiched between layers of absorber mate-
491 rial and electrodes. Liquid argon is advantageous as a calorimeter active medium due to its natural
492 abundance and low cost, chemical stability, radiation tolerance, and linear response over a large
493 energy range [21]. The calorimeter is cooled to 87k by three cryostats: one barrel cryostat encom-
494 passing the EMB, and two endcap cryostats. The barrel cryostat also encloses the solenoid which
495 produces the 2T magnetic field for the inner detector. Front-end electronics are housed outside the
496 cryostats and are used to process, temporarily store, and transfer the calorimeter signals.

497 **Electromagnetic Calorimeter**

498 For the electromagnetic calorimeters, the layers of electrodes and absorber materials are ar-
499 ranged in an an accordion shape, as illustrated in Figure 4.4. The accordion shape ensures that
500 each half barrel is continuous in the azimuthal angle, which is a key feature for ensuring consistent
501 high resolution measurements. Liquid argon permeates the space between the lead absorber plates,
502 and a multilayer copper-polymide readout board runs through the center of the liquid argon filled
503 gap.

504 The detection principle for the LAr calorimeter is the current created by electrons which are

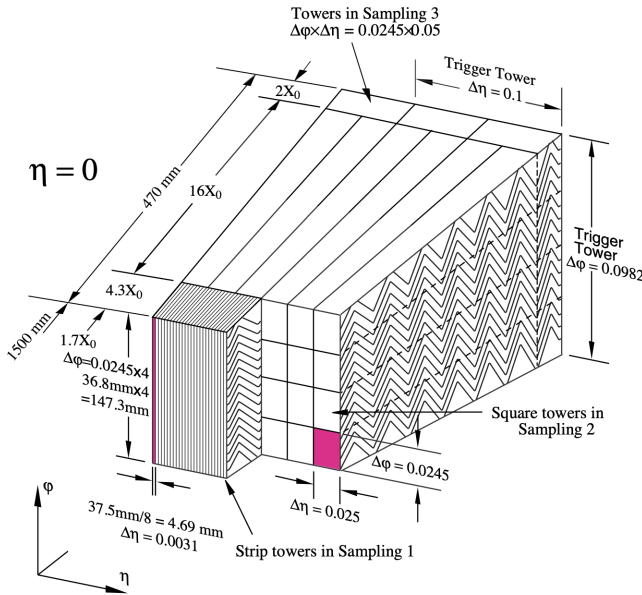


Figure 4.4: Diagram of a segment of the EMB, demonstrating the accordion plate arrangement [20]

505 released when a charged particle ionizes the liquid argon. In the barrel region, the electrons are
 506 driven towards the center electrodes by a 2000 V potential with a drift time of less than 450 ns [22].
 507 In the end-caps the voltage varies as a function of the radius in order to maintain a flat response
 508 [20]. The amount of current produced by the ionized electrons is proportional to the energy of
 509 the particle creating the signal. Figure 4.5 shows the shape of the signal produced in the LAr
 510 calorimeter, before and after it undergoes shaping during the readout process. The shaping of the
 511 pulse enforces a positive peak and a negative tail, which ensures that subsequence pulses can be
 512 separated with the precision required for the 25 ns LHC bunch spacing [20].

513 Hadronic End-cap Calorimeter

514 The HEC sits radially beyond the EMEC. The copper absorber plates in the HEC are oriented
 515 perpendicular to the beamline, with LAr as the active medium. Each end-cap is divided into two
 516 independent wheels; the inner wheel uses 25 mm copper plates, while the outer wheel uses 50 mm
 517 plates as a cost saving measure. In each wheel, the 8.5 mm plate gap is crossed by three parallel

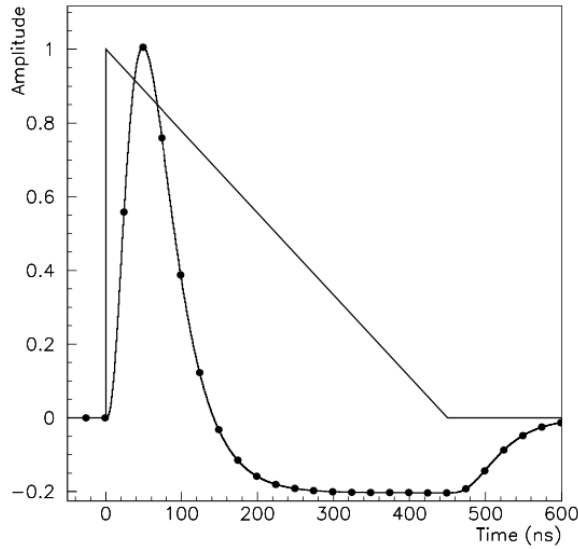


Figure 4.5: A LAr pulse as produced in the detector (triangle) and after shaping (curve) [20]

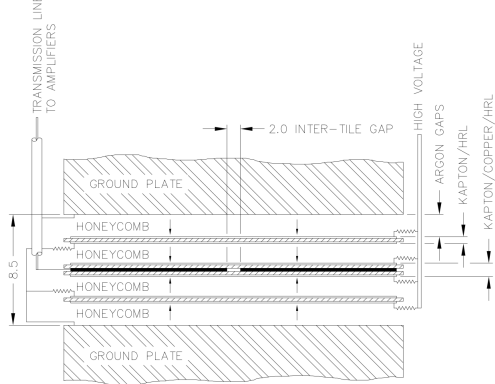


Figure 4.6: Readout gap structure in HEC [20]

518 electrodes, creating an effective drift distance of 1.8 mm. This gap is illustrated in Figure 4.6.
 519 Each wheel is divided into 32 wedge-shaped modules, each containing their own set of readout
 520 electronics.

521 **Forward Calorimeter**

522 The forward range is covered by the FCal, which provides both EM and hadronic calorimetry.
 523 It is composed of three active cylindrical modules; one EM module with copper absorber plates,
 524 and two hadronic modules with tungsten absorber plates. The plates are oriented perpendicular to

525 the beamline, and LAr is used as the active material throughout. The electrodes of the FCal consist
526 of tubes that run parallel to the beam line, arranged in a honeycomb pattern. The resulting LAr
527 gaps are as small as $250\ \mu\text{m}$, which enables the FCal to handle the large influx of particles in the
528 forward region [20].

529 4.3.2 Tile Calorimeter

530 The Tile Calorimeter (TileCal) provides hadronic calorimetry in the region $\eta < 1.7$, and sur-
531 rounds the LAr calorimeter. It is responsible for measurements of jet energy and jet substructure,
532 and also plays an important role in electron isolation and triggering (including muons) [23]. Tile-
533 Cal is composed of 3 sections, as shown in Figure 4.3; a barrel calorimeter sits directly outside the
534 LAr EMB and provides coverage up to $\eta < 1.0$. Two extended barrel sections sit outside the LAr
535 endcaps and cover the region $0.8 < \eta < 1.7$.

536 TileCal is a sampling calorimeter composed of steel and plastic scintillator plates as illustrated
537 in Figure 4.7. A total of 460,000 scintillators are read out by wavelength-shifting fibers. The
538 fibers are gathered to define cells and in turn read out by photomultiplier tubes, which amplify
539 the signal and convert it to an electrical signature. Each cell has an approximate granularity of
540 $\Delta\eta \times \Delta\phi = 0.1 \times 0.1$. Each barrel is divided azimuthally into 64 independent modules, an example
541 of which is show in Figure 4.7. The modules are each serviced by front-end electronic housed in a
542 water-cooled drawer on the exterior of the module.

543 The detection principle of the TileCal is the production of light from hadronic particles inter-
544 acting with the scintillating tiles. When a hadronic particle hits the steel plate, a shower of particles
545 are produced. The interaction of the shower with the plastic scintillator produces photons, the num-
546 ber and intensity of which are proportional to the original particle's energy.

547

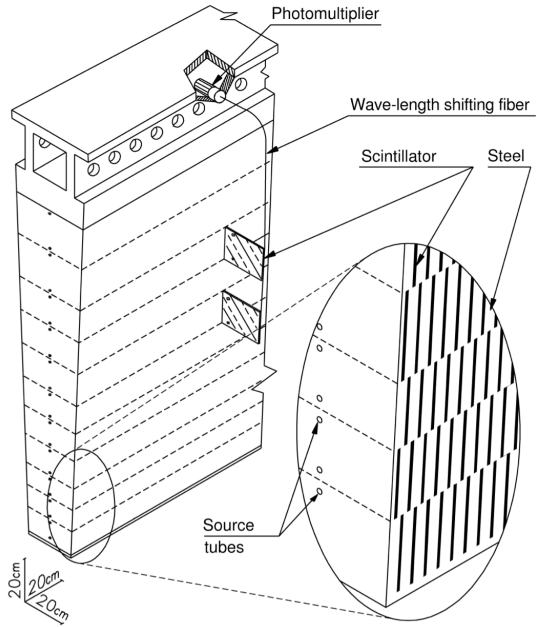


Figure 4.7: TileCal wedge module [23]

548 4.4 Muon Spectrometer

549 Unlike electrons, photons, and hadrons, muons interact minimally with the ATLAS calorimeters,
 550 and can pass through large amounts of detector material without stopping. The ATLAS Muon
 551 Spectrometer (MS) provides additional tracking information to improve the identification and mea-
 552 surement of muons. The MS comprises the outermost layers of the detector, and is interspersed
 553 with toroid magnets (discussed in Section 4.5), which provide a magnetic field of approximately
 554 0.5 T. The magnetic field bends the trajectory of the muons as they pass through the detector, and
 555 the degree of the bend is directly correlated with the muon momentum. The path of the muon is
 556 primarily measured by hits in three layers of Monitored Drift Tube (MDT) precision chambers,
 557 which cover the range $|\eta| < 2.7$. The barrel layout of the MS is show in Figure 4.8.

558 Muon triggering is provided by three layers of Resistive Plate Chambers (RPC) in the barrel
 559 ($|\eta| < 1.05$), and 3 - 4 layers of Thin Gap Chambers (TGC) in the end-caps ($1.05 < |\eta| < 2.4$).
 560 RPCs and TGCs also provide muon track measurements in the non-bending coordinate (ϕ). RPCs
 561 are constructed from two parallel resistive plates separated by a 2mm gap filled with a sensitive

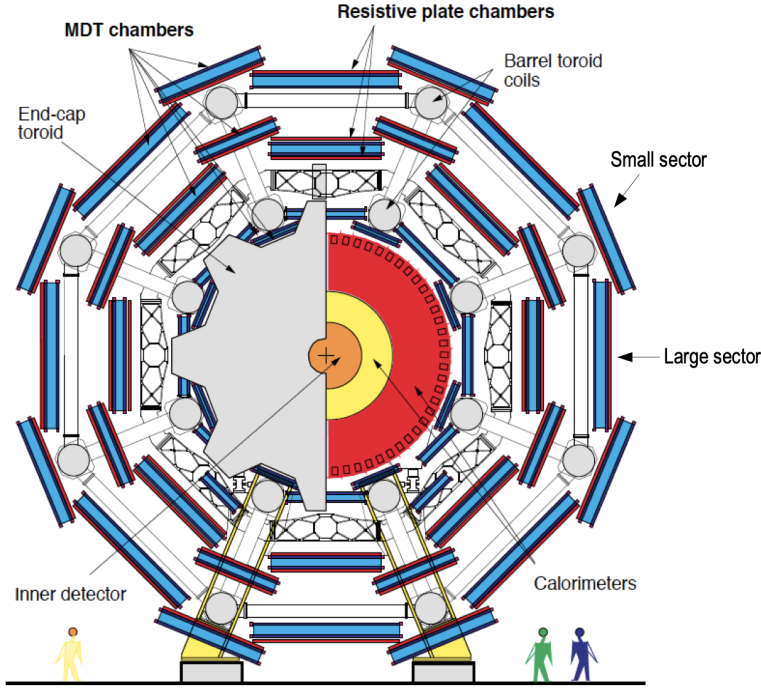


Figure 4.8: Cross section view of the muon spectrometer system [24]

gas mixture. This provides a total of six independent measurements for each muon track, with a spatial resolution of ~ 1 cm and a time resolution of ~ 1 ns. Time measurements from the RPCs are primarily associated to hits in the MDT precision chambers to determine the bunch crossing. The time measurement is also used to reject cosmic muons, and to search for delayed signals. TCGs provide triggering in the end-cap regions, and consist of parallel $30\ \mu\text{m}$ wires suspended in a sensitive gas mixture. TCGs provide high radiation tolerance and a fast response time, both features that are necessary for handling the high flux of muons in the forward region [24].

Precision measurements of muon momentum and position are primarily achieved by MDTs. The MDTs are constructed from 30 mm diameter tubes, permeated by a gas mixture of 93% Ar and 7% CO₂. The average single-tube spatial resolution is $80\ \mu\text{m}$. Each chamber consists of six drift tube layers, which together provide a muon track segment resolution of $35\ \mu\text{m}$. The momentum of the muons can be calculated from the bend in the muon trajectory as they pass through the 0.5T magnetic field provided by the toroids. For a $p_T = 1$ TeV track, the average p_T resolution is 11%. In the inner most end-cap wheels, Cathode Strip Chambers (CSC) are used instead of MDTs,

576 covering the region $2.0 < |\eta| < 2.7$. CSCs are multi-wire proportional chambers, with a cathode
577 strip readout. The CSCs have a spatial resolution in the range of $50 \mu\text{m}$, and a maximum drift time
578 of about 30 ns, which makes them superior for handling the high flux of particles in the forward
579 region [25].

580 **4.5 Magnet System**

581 The ATLAS magnet system consists of four sets of superconducting magnets: a barrel solenoid,
582 a barrel toroid, and two end-cap toroids. The solenoid magnet produces a 2T magnetic field re-
583 sponsible for bending the trajectories of charged particles as they pass through the inner detector.
584 The three toroid magnets provide a field of 0.5 - 1 T and curve the path of muons passing through
585 the muon spectrometer.

586 The inner solenoid magnet is composed of over 9 km of niobium-titanium superconductor
587 wires, which are imbedded into strengthen pure aluminum strips. The solenoid is just 4.5 cm
588 thick, which minimizes interactions between the magnet material and particles passing through the
589 detector. It is housed in the LAr cryostat, as described in section 4.3.1, which further reduces the
590 amount of non-detector material required to support the solenoid. The return yoke of the magnet
591 is provided by the iron absorber of the TileCal [26].

592 The central ATLAS toroid magnet, providing the magnetic field for the barrel region of the MS,
593 is the largest toroidal magnet ever constructed at 25 m in length. The toroid is composed of eight
594 individual coils, each housed in their own cryostat. The toroidal magnetic field is advantageous
595 as the direction of the field is almost perpendicular to the path of the charged particles. 56 km of
596 aluminum stabilized niobium-titanium-copper superconductor wire compose the magnet. In each
597 end-cap, eight smaller superconducting coils extend the toroidal magnetic field to particles leaving
598 the detector in the forward direction [26]. Figure 4.9 shows the layout of the toroid magnets.

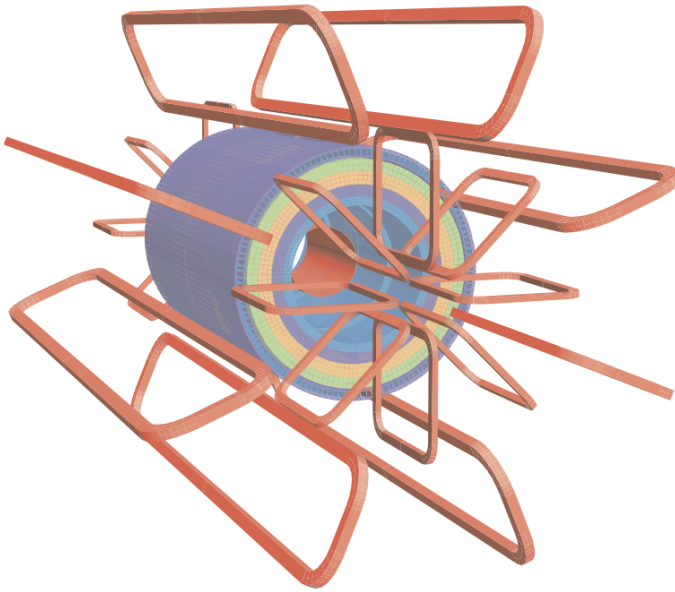


Figure 4.9: Layout of the barrel and endcap toroid magnets [17]

599 4.6 Forward Detectors

600 In addition to the inner detector, calorimeters, and muon spectrometer, three smaller detectors
601 provide coverage in the very forward region. The innermost forward detector, at 17 m from the
602 interaction point, is the **L**Uminosity measurement using **C**erenkov **I**ntegrating **D**etector (LUCID).
603 LUCID's primary purpose is to measure the relative online-luminosity for the ATLAS detector,
604 from inelastic $p - p$ scattering. The detector is composed of 20 aluminum Cerenkov tubes which
605 surround the beam pipe and face towards the interaction point.

606 The second forward detector is the Zero-Degree Calorimeter (ZDC), located 140 m from the
607 interaction point in both directions, at the point where the LHC beam-pipe divides into two separate
608 pipes. The ZDC's primary purpose is to detect forward neutrons from heavy ion collisions.

609 The third forward detector is the Absolute Luminosity For ATLAS (ALFA) system, located 240
610 m from the interaction point in both directions. ALFA determines luminosity by measuring elastic
611 scattering at small angles, from which luminosity can be calculated via the optical theorem. The
612 detector is built from scintillating fiber trackers. These are connected to the accelerator vacuum

613 via Roman pots, which allow the detector to come as close as 1mm to the beam without disrupting
614 the machine vacuum. The LUCID and ALFA detectors are crucial to determining the real-time
615 conditions of the beams and the total luminosity delivered to the ATLAS detector [17].

616 **4.7 Trigger and Data Acquisition**

617 The trigger and Data Acquisition systems (TDAQ) are responsible for selecting the most viable
618 events to save for further downstream processing. Because of the high luminosities delivered to
619 the ATLAS detector, not all events recorded can be saved; the 40 MHz bunch crossing rate must
620 be reduced by 5 orders of magnitude to an event storage rate of ~ 1 kHz. The trigger system is
621 composed of three distinct levels: Level 1 (L1), Level 2 (L2) and the event filter. Collectively the
622 L2 trigger and the event filter form the High Level Trigger (HLT).

623 The L1 trigger is implemented in the hardware of the ATLAS calorimeter and muon systems.
624 The primary modality of the L1 trigger is to identify muons, electrons, photons, jets, and τ -leptons
625 with high transverse momentum. Particles with high transverse momentum are more likely to
626 originate from direct, high energy collisions, which are most likely to produce interesting physics
627 processes. The L1 trigger also identifies events with large missing transverse energy, which could
628 be indicative of new physics. The L1 muon trigger (L1Muon) relies on RPC and TGC trigger
629 chambers in the barrel and end-cap regions of the muon spectrometer. The L1 Calorimeter Trigger
630 (L1Calo) uses reduced granularity information collected by all the calorimeter subsystems. Results
631 from the L1Muon and L1Calo triggers are combined by the Central Trigger Processor (CTP),
632 which implements a trigger ‘menu’, listing various combinations of trigger requirements. The
633 maximum L1 acceptance rate is 75 kHz, and the L1 trigger decision must reach the front-end
634 electronics within $2.5 \mu\text{s}$ of its associated bunch-crossing [17].

635 The L1 trigger defines a Region-of-Interest (RoI) for each passing event. The ROI is repre-
636 sented by the η - ϕ detector region where interesting features were identified by the L1 selection
637 process. Information about the type of feature identified and the threshold which was exceeded to
638 trigger the L1 response is also recorded. The ROI data is sent to the L2 trigger, which uses all of

639 the available information within the ROI at full granularity and precision. The L2 trigger reduces
640 the event rate from 75 kHz to 3.5 kHz, with an average processing time of 40 ms. The final stage of
641 the HLT is the event filter, which reduces the event rate to 200 Hz. The event filter uses an offline
642 analysis process to select fully rebuilt events which will be saved for further analysis.

643 All levels of the ATLAS trigger system depend on specialized electronics. Each detector front-
644 end system has a specialized Readout Driver (ROD) which collects information from several front-
645 end data streams at once. The ROD is composed of front-end analogue processing, an L1 buffer
646 which retains the information long enough for the L1 trigger decision, and dedicated links which
647 send the front-end L1 triggered data to Data Acquisition System (DAQ). Any digital signals are
648 formatted as raw data before being transferred to the DAQ. The first stage of the DAQ temporarily
649 stores the L1 data in local buffers. The ROI data is then requested by the L2 trigger, after which
650 selected events are transferred to an event building system, before events passing the event filter
651 are sent to the CERN computer center for permanent storage. The DAQ system not only allows
652 for the readout of detector data, but is also responsible for the monitoring and configuration of
653 the hardware and software components which make up the data readout system via the Detector
654 Control System (DCS).

655 The DCS allows centralized control of all detector subsystems simultaneously. It continually
656 monitors operational conditions, reports any abnormal behavior to the operator, and can perform
657 both automatic and manual interventions. The DCS reports on real time detector conditions such
658 as high or low voltage detector electronics, gas and cooling systems, magnetic field conditions,
659 humidity and temperature. This information is continually monitored by experts in the ATLAS
660 control room, so that action can be taken immediately to correct any issues that arise. The DCS also
661 handles communication between detector systems, and other systems such as the LHC accelerator,
662 the ATLAS magnets, and CERN technical services [17].

Chapter 5: Particle Reconstruction and Identification

665 Lorem ipsum dolor sit amet, consectetur adipiscing elit, sed do eiusmod tempor incididunt ut
666 labore et dolore magna aliqua. Ut enim ad minim veniam, quis nostrud exercitation ullamco laboris
667 nisi ut aliquip ex ea commodo consequat. Duis aute irure dolor in reprehenderit in voluptate velit
668 esse cillum dolore eu fugiat nulla pariatur. Excepteur sint occaecat cupidatat non proident, sunt in
669 culpa qui officia deserunt mollit anim id est laborum.. Lorem ipsum dolor sit amet, consectetur
670 adipiscing elit, sed do eiusmod tempor incididunt ut labore et dolore magna aliqua. Ut enim ad
671 minim veniam, quis nostrud exercitation ullamco laboris nisi ut aliquip ex ea commodo consequat.
672 Duis aute irure dolor in reprehenderit in voluptate velit esse cillum dolore eu fugiat nulla pariatur.
673 Excepteur sint occaecat cupidatat non proident, sunt in culpa qui officia deserunt mollit anim id est
674 laborum..

Conclusion or Epilogue

676 Use this page for your epilogue or conclusion if applicable; please use only one of the titles
677 for this page. Otherwise, you may delete it. Use this page for your epilogue or conclusion if
678 applicable; please use only one of the titles for this page. Otherwise, you may delete it. Use this
679 page for your epilogue or conclusion if applicable; please use only one of the titles for this page.
680 Otherwise, you may delete it. Use this page for your epilogue or conclusion if applicable; please
681 use only one of the titles for this page. Otherwise, you may delete it. Use this page for your
682 epilogue or conclusion if applicable; please use only one of the titles for this page. Otherwise,
683 you may delete it. Use this page for your epilogue or conclusion if applicable; please use only one
684 of the titles for this page. Otherwise, you may delete it. Use this page for your epilogue or
685 conclusion if applicable; please use only one of the titles for this page. Otherwise, you may delete
686 it. Use this page for your epilogue or conclusion if applicable; please use only one of the titles for
687 this page. Otherwise, you may delete it. Use this page for your epilogue or conclusion if
688 applicable; please use only one of the titles for this page. Otherwise, you may delete it. Use this
689 page for your epilogue or conclusion if applicable; please use only one of the titles for this page.
690 Otherwise, you may delete it. Use this page for your epilogue or conclusion if applicable; please
691 use only one of the titles for this page. Otherwise, you may delete it. Use this page for your
692 epilogue or conclusion if applicable; please use only one of the titles for this page. Otherwise,
693 you may delete it. Use this page for your epilogue or conclusion if applicable; please use only one
694 of the titles for this page. Otherwise, you may delete it. Use this page for your epilogue or
695 conclusion if applicable; please use only one of the titles for this page. Otherwise, you may delete

696 it. Use this page for your epilogue or conclusion if applicable; please use only one of the titles for
697 this page. Otherwise, you may delete it. Use this page for your epilogue or conclusion if
698 applicable; please use only one of the titles for this page. Otherwise, you may delete it. Use this
699 page for your epilogue or conclusion if applicable; please use only one of the titles for this page.
700 Otherwise, you may delete it. Use this page for your epilogue or conclusion if applicable; please
701 use only one of the titles for this page. Otherwise, you may delete it. Use this page for your
702 epilogue or conclusion if applicable; please use only one of the titles for this page. Otherwise,
703 you may delete it. Use this page for your epilogue or conclusion if applicable; please use only one
704 of the titles for this page. Otherwise, you may delete it. Use this page for your epilogue or
705 conclusion if applicable; please use only one of the titles for this page. Otherwise, you may delete
706 it. Use this page for your epilogue or conclusion if applicable; please use only one of the titles for
707 this page. Otherwise, you may delete it. Use this page for your epilogue or conclusion if
708 applicable; please use only one of the titles for this page. Otherwise, you may delete it. Use this
709 page for your epilogue or conclusion if applicable; please use only one of the titles for this page.
710 Otherwise, you may delete it. Use this page for your epilogue or conclusion if applicable; please
711 use only one of the titles for this page. Otherwise, you may delete it. Use this page for your
712 epilogue or conclusion if applicable; please use only one of the titles for this page. Otherwise,
713 you may delete it. Use this page for your epilogue or conclusion if applicable; please use only one
714 of the titles for this page. Otherwise, you may delete it. Use this page for your epilogue or
715 conclusion if applicable; please use only one of the titles for this page. Otherwise, you may delete
716 it. Use this page for your epilogue or conclusion if applicable; please use only one of the titles for
717 this page. Otherwise, you may delete it. Use this page for your epilogue or conclusion if
718 applicable; please use only one of the titles for this page. Otherwise, you may delete it. Use this
719 page for your epilogue or conclusion if applicable; please use only one of the titles for this page.
720 Otherwise, you may delete it. Use this page for your epilogue or conclusion if applicable; please
721 use only one of the titles for this page. Otherwise, you may delete it. Use this page for your
722 epilogue or conclusion if applicable; please use only one of the titles for this page. Otherwise,

723 you may delete it. Use this page for your epilogue or conclusion if applicable; please use only one
724 of the titles for this page. Otherwise, you may delete it. Use this page for your epilogue or
725 conclusion if applicable; please use only one of the titles for this page. Otherwise, you may delete
726 it. Use this page for your epilogue or conclusion if applicable; please use only one of the titles for
727 this page. Otherwise, you may delete it. Use this page for your epilogue or conclusion if
728 applicable; please use only one of the titles for this page. Otherwise, you may delete it. Use this
729 page for your epilogue or conclusion if applicable; please use only one of the titles for this page.
730 Otherwise, you may delete it. Use this page for your epilogue or conclusion if applicable; please
731 use only one of the titles for this page. Otherwise, you may delete it. Use this page for your
732 epilogue or conclusion if applicable; please use only one of the titles for this page. Otherwise,
733 you may delete it. Use this page for your epilogue or conclusion if applicable; please use only one
734 of the titles for this page. Otherwise, you may delete it. Use this page for your epilogue or
735 conclusion if applicable; please use only one of the titles for this page. Otherwise, you may delete
736 it. Use this page for your epilogue or conclusion if applicable; please use only one of the titles for
737 this page. Otherwise, you may delete it. Use this page for your epilogue or conclusion if
738 applicable; please use only one of the titles for this page. Otherwise, you may delete it. Use this
739 page for your epilogue or conclusion if applicable; please use only one of the titles for this page.
740 Otherwise, you may delete it. Use this page for your epilogue or conclusion if applicable; please
741 use only one of the titles for this page. Otherwise, you may delete it. Use this page for your
742 epilogue or conclusion if applicable; please use only one of the titles for this page. Otherwise,
743 you may delete it. Use this page for your epilogue or conclusion if applicable; please use only one
744 of the titles for this page. Otherwise, you may delete it. Use this page for your epilogue or
745 conclusion if applicable; please use only one of the titles for this page. Otherwise, you may delete
746 it. Use this page for your epilogue or conclusion if applicable; please use only one of the titles for
747 this page. Otherwise, you may delete it. Use this page for your epilogue or conclusion if
748 applicable; please use only one of the titles for this page. Otherwise, you may delete it. Use this
749 page for your epilogue or conclusion if applicable; please use only one of the titles for this page.

750 Otherwise, you may delete it. Use this page for your epilogue or conclusion if applicable; please
751 use only one of the titles for this page. Otherwise, you may delete it. Use this page for your
752 epilogue or conclusion if applicable; please use only one of the titles for this page. Otherwise,
753 you may delete it. Use this page for your epilogue or conclusion if applicable; please use only one
754 of the titles for this page. Otherwise, you may delete it. Use this page for your epilogue or
755 conclusion if applicable; please use only one of the titles for this page. Otherwise, you may delete
756 it. Use this page for your epilogue or conclusion if applicable; please use only one of the titles for
757 this page. Otherwise, you may delete it. Use this page for your epilogue or conclusion if
758 applicable; please use only one of the titles for this page. Otherwise, you may delete it. Use this
759 page for your epilogue or conclusion if applicable; please use only one of the titles for this page.
760 Otherwise, you may delete it. Use this page for your epilogue or conclusion if applicable; please
761 use only one of the titles for this page. Otherwise, you may delete it. Use this page for your
762 epilogue or conclusion if applicable; please use only one of the titles for this page. Otherwise,
763 you may delete it. Use this page for your epilogue or conclusion if applicable; please use only one
764 of the titles for this page. Otherwise, you may delete it. Use this page for your epilogue or
765 conclusion if applicable; please use only one of the titles for this page. Otherwise, you may delete
766 it. Use this page for your epilogue or conclusion if applicable; please use only one of the titles for
767 this page. Otherwise, you may delete it. Use this page for your epilogue or conclusion if
768 applicable; please use only one of the titles for this page. Otherwise, you may delete it. Use this
769 page for your epilogue or conclusion if applicable; please use only one of the titles for this page.
770 Otherwise, you may delete it. Use this page for your epilogue or conclusion if applicable; please
771 use only one of the titles for this page. Otherwise, you may delete it. Use this page for your
772 epilogue or conclusion if applicable; please use only one of the titles for this page. Otherwise,
773 you may delete it. Use this page for your epilogue or conclusion if applicable; please use only one
774 of the titles for this page. Otherwise, you may delete it. Use this page for your epilogue or
775 conclusion if applicable; please use only one of the titles for this page. Otherwise, you may delete
776 it.

References

- [1] David J Griffiths. *Introduction to elementary particles; 2nd rev. version.* Physics textbook. New York, NY: Wiley, 2008.
- [2] M. Tanabashi et al. “Review of Particle Physics”. In: *Phys. Rev. D* 98 (3 2018), pp. 847–851.
- [3] J. E. Augustin et al. “Discovery of a Narrow Resonance in e^+e^- Annihilation”. In: *Phys. Rev. Lett.* 33 (1974), pp. 1406–1408.
- [4] J. J. Aubert et al. “Experimental Observation of a Heavy Particle J ”. In: *Phys. Rev. Lett.* 33 (1974), pp. 1404–1406.
- [5] Martin L. Perl et al. “Evidence for Anomalous Lepton Production in e+ - e- Annihilation”. In: *Phys. Rev. Lett.* 35 (1975), pp. 1489–1492.
- [6] Lyndon Evans and Philip Bryant. “LHC Machine”. In: *Journal of Instrumentation* 3.08 (2008), S08001.
- [7] “The ATLAS Experiment at the CERN Large Hadron Collider”. In: *JINST* 3 (2008). Also published by CERN Geneva in 2010, S08003.
- [8] “The CMS experiment at the CERN LHC”. In: *Journal of Instrumentation* 3.08 (2008), S08004.
- [9] “The ALICE experiment at the CERN LHC”. In: *Journal of Instrumentation* 3.08 (2008), S08002.
- [10] “The LHCb Detector at the LHC”. In: *Journal of Instrumentation* 3.08 (2008), S08005.
- [11] Ana Lopes and Melissa Loyse Perrey. *FAQ-LHC The guide*. 2022.
- [12] Esma Mobs. “The CERN accelerator complex in 2019. Complexe des accélérateurs du CERN en 2019”. In: (2019). General Photo.
- [13] *Pulling together: Super Conducting electromagnets*. <https://home.cern/science/engineering/pulling-together-superconducting-electromagnets>. Accessed: 2024-01-05.
- [14] *The High-Luminosity LHC*. <https://voisins.web.cern.ch/en/high-luminosity-lhc-hl-lhc>. Accessed: 2024-01-05.

- 804 [15] Aad G., et al. (ATLAS Collaboration and CMS Collaboration). “Combined Measurement of
805 the Higgs Boson Mass in pp Collisions at $\sqrt{s} = 7$ and 8 TeV with the ATLAS and CMS
806 Experiments”. In: *Phys. Rev. Lett.* 114 (19 2015), p. 191803.
- 807 [16] O. Aberle et al. *High-Luminosity Large Hadron Collider (HL-LHC): Technical design re-*
808 *port.* CERN Yellow Reports: Monographs. Geneva: CERN, 2020.
- 809 [17] The ATLAS Collaboration. “The ATLAS Experiment at the CERN Large Hadron Collider”.
810 In: *Journal of Instrumentation* 3.08 (2008), S08003.
- 811 [18] G Aad, B Abbott, and ATLAS Collaboration. “Performance of the reconstruction of large
812 impact parameter tracks in the inner detector of ATLAS”. In: *Eur. Phys. J. C Part. Fields*
813 83.11 (Nov. 2023).
- 814 [19] Joao Pequenao. *Computer Generated image of the ATLAS calorimeter*. 2008.
- 815 [20] *ATLAS liquid-argon calorimeter: Technical Design Report*. Technical design report. AT-
816 LAS. Geneva: CERN, 1996.
- 817 [21] H A Gordon. “Liquid argon calorimetry for the SSC”. In: () .
- 818 [22] Henric Wilkens and (on behalf ofthe ATLAS LArg Collaboration). “The ATLAS Liquid
819 Argon calorimeter: An overview”. In: *Journal of Physics: Conference Series* 160.1 (2009),
820 p. 012043.
- 821 [23] *Technical Design Report for the Phase-II Upgrade of the ATLAS Tile Calorimeter*. Tech.
822 rep. Geneva: CERN, 2017.
- 823 [24] “Technical Design Report for the Phase-II Upgrade of the ATLAS Muon Spectrometer”. In:
824 () .
- 825 [25] L Pontecorvo. “The ATLAS Muon Spectrometer”. In: (2004). revised version number 1
826 submitted on 2003-07-27 16:31:16.
- 827 [26] *ATLAS magnet system: Technical Design Report, 1*. Technical design report. ATLAS. Geneva:
828 CERN, 1997.

Appendix A: Experimental Equipment

831 Lorem ipsum dolor sit amet, consectetur adipiscing elit, sed do eiusmod tempor incididunt ut
832 labore et dolore magna aliqua. Ut enim ad minim veniam, quis nostrud exercitation ullamco laboris
833 nisi ut aliquip ex ea commodo consequat. Duis aute irure dolor in reprehenderit in voluptate velit
834 esse cillum dolore eu fugiat nulla pariatur. Excepteur sint occaecat cupidatat non proident, sunt in
835 culpa qui officia deserunt mollit anim id est laborum.

Appendix B: Data Processing

838 Lorem ipsum dolor sit amet, consectetur adipiscing elit, sed do eiusmod tempor incididunt ut
839 labore et dolore magna aliqua. Ut enim ad minim veniam, quis nostrud exercitation ullamco laboris
840 nisi ut aliquip ex ea commodo consequat. Duis aute irure dolor in reprehenderit in voluptate velit
841 esse cillum dolore eu fugiat nulla pariatur. Excepteur sint occaecat cupidatat non proident, sunt in
842 culpa qui officia deserunt mollit anim id est laborum.